

LAP: An Attention-Based Module for Faithful Interpretation and Knowledge Injection in Convolutional Neural Networks

Rassa Ghavami Modegh^{*,1,2,3}, Ahmad Salimi^{*,2,3}, Hamid R. Rabiee^{**,1,2,3}

¹DML, Department of Computer Engineering, Sharif University of Technology, Tehran, Iran

²AI-Med Group, AI Innovation Center, Sharif University of Technology, Tehran, Iran

³Department of Computer Engineering, Sharif University of Technology, Tehran, Iran

Abstract—Despite the state-of-the-art performance of deep convolutional neural networks, they are susceptible to bias and malfunction in unseen situations. The complex computation behind their reasoning is not sufficiently human-understandable to develop trust. External explainer methods have tried to interpret the network decisions in a human-understandable way, but they are accused of fallacies due to their assumptions and simplifications. On the other side, the inherent self-interpretability of models, while being more robust to the mentioned fallacies, cannot be applied to the already trained models. In this work, we propose a new attention-based pooling layer, called Local Attention Pooling (LAP), that accomplishes self-interpretability and the possibility for knowledge injection while improving the model's performance. Moreover, several weakly-supervised knowledge injection methodologies are provided to enhance the process of training. We verified our claims by evaluating several LAP-extended models on three different datasets, including Imagenet. The proposed framework offers more valid human-understandable and more faithful-to-the-model interpretations than the commonly used white-box explainer methods.

I. INTRODUCTION

As Artificial Intelligence (AI) proved its efficiency and superior-than-humans performance in many fields, its applications have been expanded. Nowadays, AI has entered into real-life applications like clinical computer-aided decision systems, medical diagnosis, and autonomous car driving. These critical applications arose the question of whether AI models are trustable and their decisions are valid. Deep Neural Networks (DNNs), as one of the most successful AI models, make their decisions by complex computations which are not understandable by humans. They are trained in an end-to-end fashion and are susceptible to learning detours and biases of the dataset rather than the actual concepts and reasons. Since AI has become responsible for making decisions in areas interfering with human rights and ethics, governments have started to make laws about its usages. For example, the European Union has adopted new regulations which enable users to demand an explanation of an algorithmic decision that has affected them [13]. This has strengthened the urge for DNNs to explain themselves. Explaining DNNs have other virtues besides verification of decisions, bias detection, developing trust, and compliance to legislation [5]; it can help in diagnosing the model. Also, knowledge can be discovered from the models with superior-than-human performance to enrich human knowledge [9].

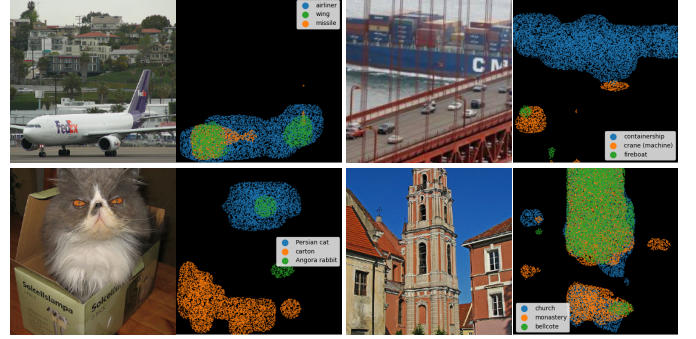


Fig. 1. Examples of concept-wise interpretations of a LAP-extended Model.

In recent years, there have been many attempts in providing explanations and interpretations for DNNs' decisions. These studies can be divided into two general areas of intrinsic and post-hoc methods. Intrinsic interpretability is achieved by enforcing interpretability into the model's architecture [30], [38], [41] and the training strategy [8], [10], [17], [41]. In this approach, the model itself can provide explanations for its decisions. These methods do not apply to already trained models [12], [16]. They generally pose limitations over the model's architecture, and some may sacrifice the performance to achieve interpretability [12]. Post-hoc methods try to provide explanations for already trained models. They adopt assumptions and simplifications in their computations that may sacrifice fidelity to achieve more human-understandable explanations [12]. These assumptions also may lead to false interpretations as they may not be valid in the model's decision-making process [34].

Attention-based architectures are a type of intrinsically interpretable architectures. Attention was first used in Natural Language Processing (NLP) to enable a word to take effect from any of the sentence's words without being restricted to their distance [3]. It could provide a score over the words to highlight which words are more important in deciding about another word. Later its applications extended to the field of vision to mimic human attention in tasks such as visual question answering [21] and image captioning [40]. In general, attention provides an importance score over all of the input tokens. In this work, we utilize the attention mechanism to propose a new pooling layer, easily pluggable into any convolutional neural network (CNN). Our main contributions can be summarized as follows:

- Introducing a new module that is easily pluggable to

*Equal contribution

**Corresponding author: rabiee@sharif.edu

any CNN, including the already trained networks, that accommodate the model with self-interpretability and the possibility to inject knowledge without restricting the architecture, performance loss, adding parameters to the main-stream of information flow, and increasing order of computations

- Proposing a concept-wise attention mechanism that assigns attention scores to any predefined domain concepts to distinguish the importance of each pixel according to each concept (Fig. 1)
- Proposing a weakly supervised method for injecting knowledge into the model, useful in shaping the decision-making process of the model leading to more interpretability

II. RELATED WORKS

A. Importance based pooling

Pooling layers and strided convolutions are widely used in CNNs to increase the receptive field and decrease memory consumption. Gao et al. have proposed a unified framework for formulating different pooling strategies and a pooling method called Local Importance Pooling (LIP) [11]. In this framework, features within local sliding windows are aggregated by weighted averaging. The weights are assigned based on the importance of the features. According to this framework, average pooling assumes the same importance score for all the pixels and is susceptible to feature fading. Max pooling assigns one to the highest feature and zeroes to all the others, leading to very sparse gradient paths and slow training. Strided convolutions assign importance based on the pixel's location in the window and are more sensitive to shift variances. LIP has used the attention mechanism to assign importance weights to the features. LIP is applied in a feature-wise manner which makes it different from our proposed architecture. All of the mentioned pooling layers except strided convolutions can lead to loss of relative spatial relations, as they select different features from different spatial locations [26].

B. Explainability methods

In recent years, many studies have been published about the interpretability and explainability of DNNs. Some of the proposed methods are model-agnostic and treat models as black-boxes. These methods either mimic the operations of the black-box by training a white-box model and interpreting it instead [37], which is susceptible to errors as the mimicked model does not perform exactly as the main model. Another group of model-agnostic methods like LIME [28] assesses feature sensitivity by perturbing the feature space around each input which demands an optimization per sample and is computationally inefficient for being applied on many samples with large feature spaces like images.

Model-specific methods work on specific white-box models, meaning they use the architecture and parameters of the model to provide explanations. Gradient-based methods belong to this group. They use gradients of class scores w.r.t the input to find the most sensitive features as if the network is estimated with a Taylor series of order one. The gradients are the weights

of the features indicating their importance. Vanilla gradient [33] has used the pure gradients to find important features. It produces a noisy importance map. Guided Backpropagation [35] filters negative gradient flows to bold out the effective pixels. This may lead to false positives. Grad-CAM [31] uses gradients to find the importance of channels and then calculates pixel scores based on their channel-wise activations and the channel importance. Guided Grad-CAM [31] is a multiplication of Guided Backpropagation and Grad-Cam to produce fine-grained importance maps. All of the gradient-based methods suffer from gradient saturation problems leading to near-zero importance scores. Score-based methods like Layer-wise Relevance Propagation (LRP) [4] and Deep Lift [32] propagate scores instead of gradients to calculate the importance of pixels. Deep Lift calculates scores based on the difference of scores achieved compared to a baseline. But it is not easy to define a suitable meaningful baseline for all applications.

C. Explainability by Attention Map Visualization

Attention maps generated by attention mechanisms generally can be used to explain the model's behavior. This kind of explanation is widely used on Vision Transformers [19]. Yang et al. used Transformer raw attention maps to explain their Human Pose Estimation method [39]. Abnar et al. proposed two methods to aggregate the Transformer's attention maps to produce attention flow and attention rollout explanation maps [2]. Chefer et al. proposed an explainability method in which relevancy is assigned to attention maps and then propagated throughout all blocks [7]. Mondal et al. used this relevancy propagation method to make their COVID-19 screening system explainable [23]. Recently, Chefer et al. proposed another explanation method based on relevancy propagation [6]. In contrast to their previous work that was only applicable on Transformer encoders, this method is applicable in all transformer architectures like generative models. For CNNs, Zhang et al. [42] and Gu et al. [14] used self-attention layers inside CNN models to explain their medical image analysis systems.

III. METHOD

A. Local Attention Pool

In general, the attention mechanism conveys the information about the most important parts of the input data. We adopt the attention mechanism in the reduction process of the pooling layers. The process is depicted in Fig. 2. In contrast to LIP, the attention is not applied in a channel-wise manner. Instead, the whole feature map is passed to a scoring module to calculate pixel-wise importance scores. Then for each kernel position, the scores related to the pixels under the kernel are normalized. The final feature vector is obtained by weighted averaging the feature vectors of the pixels. This process mimics a zooming action. Instead of mixing the features of the pixels applied to a pooling kernel, the network dynamically detects the most important pixels and passes their features instead. In this way, the small and yet important details are not faded or lost, but propagated through the network's depth.

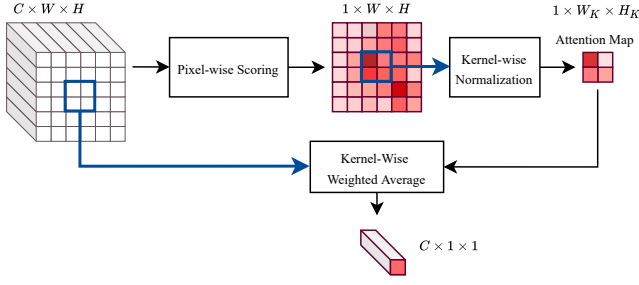


Fig. 2. The local attention pooling is applied on a kernel of size $W_K \times H_K$ on the input feature map.

It also prevents fallacies produced by feature mixing. Different zooming locations under each kernel position may also help in making the model more robust toward shifts and scales.

Interpretability is one of the well-known benefits of the attention mechanism. Attention scores identify the relative importance of each part of the input. Although any arbitrary scoring module can be used for this purpose, relative importance cannot be interpreted in an absolute way. To achieve this, we have adopted a sigmoid function at the end of the scoring module. In this way, its output can be interpreted as the importance probability of each pixel. One can adopt any arbitrary method, such as softmax, to normalize the importance scores locally based on the scores of the pixels under the kernel at each position. We have adopted the normalization function:

$$g(P_{ij}) = e^{-\alpha^2(\max\{P_{ij}\} - P_{ij})^2} \times P_{ij} + \epsilon. \quad (1)$$

In this function, P_{ij} is the vector of pixels' probabilities under the kernel at position (i, j) . The importance probabilities are multiplied by a factor derived from the Gaussian kernel around the highest local importance probability. So the sensitivity toward the most highlighted local pixel becomes adjustable by the trainable parameter α . Theoretically, $\alpha \rightarrow 0$ is equivalent to average pooling, and $\alpha \rightarrow \infty$ is equivalent to conveying the features of the most highlighted local pixel directly. We have added a small value ϵ to prevent the weights from becoming 0. This helps preserving the gradient flow to all pixels and prevents zero division in the normalization process.

B. Self-interpretability by LAP

CNNs are generally a stack of layers, most of which work by sliding a kernel all over the input and calculating a function. Although the shallower layers have lower receptive fields, they are known to extract fine common details like edges and corners. As the depth increases, the receptive field increases and the layers become responsible for extracting higher-level concepts [24]. The final decision is made based on the information flow through the layers, and somewhere in the middle, it should have understood the distinguishing concepts. LAP helps in specifying those concepts besides keeping them bold in the pooling processes. As the importance is identified based on the internal forward flow of the network, LAP modules make the model self-interpretable. LAPs do not produce false positives or negatives due to ignored flows to reach a human-understandable interpretation in contrast to

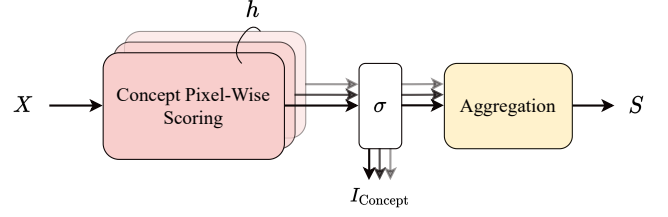


Fig. 3. Multi-concept scoring module.

external explainer methods. They also find the important parts in the same direction that the model decides in the forward process. Therefore, mistakes due to importance calculation using other directions are not made.

C. Knowledge injection

Human experts make their decisions based on special features of the input. For example, jaggedness is one of the factors considered in classifying a tumor as benign or malignant. The neural networks trained freely may or may not have considered all of the reasons in their decision making. They may have become biased to a dominant feature in the training dataset and lose generalization. LAP provides an easy way for injecting experts' knowledge into the network due to the probabilistic behavior of its scoring module. Experts can highlight the parts of the input that are important for their decision-making. The highlighted map can be resized to each LAP's input and used as ground truth to train its scoring module. Knowledge injection gives a better guarantee that the network decides based on the factors of the domain. In addition, it injects gradient to the shallower layers and makes the training process faster and better.

In general, deep models should learn one or more problem-specific concepts to do their tasks. To make the concepts distinguishable by LAPs in the network, the architecture presented in Fig. 3 can be used for the scoring module. In this architecture, there are h heads, each for scoring the corresponding concept. A sigmoid function is applied over the scores providing concept-wise importance probabilities, I_{Concept} . The importance probabilities are then aggregated to calculate the final score S . Experts' knowledge can be used to train each I_{Concept} in a supervised manner.

In most situations, we do not have detailed experts' supervision, but we have a general knowledge about the problem. So the LAP modules can be trained in a weakly supervised manner to behave as desired. Therefore it will also benefit from the gradient injection and fast training. Here, we have used a linear combination of the semi-supervised losses and the main task's loss to train the models, as described in the following.

1) *Concept-discrimination loss*: For adopting the mentioned loss, we use the design presented in Fig. 3 for the scoring module, with h concept heads. We assume each sample s has a set of concepts C_s . Each concept head highlights the important pixels for the concept, called concept-related clues. To train the concept heads, we consider the following loss terms:

Min Active Ratio (MinAR). Each concept head should assign high importance probability to at least a specified portion of the pixels in the samples containing the concept. This makes the model highlight the concept-related clues for the sample.

Max Active Ratio (MaxAR). Each concept head should assign high importance probability to at most a specified portion of the pixels in the samples containing the concept, as the main clue is not understandable otherwise. This phenomenon may happen in layers with large receptive fields. As the concept-related clue appears in the receptive fields of all of the pixels, the network may consider all of them as concept-related clues.

Inactive Ratio (IAR). Each concept head should assign low importance probability to all the pixels of the samples not containing the concept, as the concept-related clue should not exist in them. This loss can be applied to all the pixels. But because generally, most of the pixels are already inactive in the attention map, this loss term is likely to fade. Therefore, it is better to apply this term on top-scored pixels according to IAR.

Consider a LAP module l with an input size $H \times W$. The loss function for this LAP is shown in Eq. (2). In this equation, N_c and $N_{\bar{c}}$ are the number of samples containing and not containing concept c , respectively. $k_1 = \lceil \text{MinAR} \times HW \rceil$ and $k_2 = \lceil (1 - \text{MaxAR}) HW \rceil$ are the numbers of pixels encouraged to have respectively high and low probabilities in the in the samples containing concept c , and $k_3 = \lceil \text{IAR} \times HW \rceil$ is the number of top pixel encouraged to be inactive in other samples. $\text{top}_{s,k_1}^{l,c}$ and $\text{bot}_{s,k_2}^{l,c}$ are the sets of pixels of the k_1 high-ranked and k_2 low-ranked pixels of sample s based on the importance probability of concept head c . $p_{s,i,j}^{l,c}$ is the probability of concept head c for the pixel (i, j) of sample s . MinAR, MaxAR, and IAR are hyper-parameters. The first term is multiplied by 2 to balance the effect of positive and negative losses to the concept head c .

$$\begin{aligned}
& - \sum_{c=1}^h \left[\frac{2}{N_c} \sum_{s; c \in C_s} \left[\frac{1}{k_1} \sum_{(i,j) \in \text{top}_{s,k_1}^{l,c}} \ln(p_{s,i,j}^{l,c}) \right] + \right. \\
& \quad \frac{1}{N_c} \sum_{s; c \in C_s} \left[\frac{1}{k_2} \sum_{(i,j) \in \text{bot}_{s,k_2}^{l,c}} \ln(1 - p_{s,i,j}^{l,c}) \right] + \quad (2) \\
& \quad \left. \frac{1}{N_{\bar{c}}} \sum_{s; c \notin C_s} \left[\frac{1}{k_3} \sum_{(i,j) \in \text{top}_{s,k_3}^{l,c}} \ln(1 - p_{s,i,j}^{l,c}) \right] \right]
\end{aligned}$$

We observed in our experiments that choosing $\text{top}_{s,k}^{l,c}$ and $\text{bot}_{s,k}^{l,c}$ sets based on the probabilities assigned by concept head, is sensitive to the initial model parameters. If high weight is considered for concept-discrimination loss, it is likely to get stuck in considering a wrong zone in layers with high receptive fields. To prevent this, we used another module with the same architecture as the scoring module to choose $\text{top}_{s,k}^{l,c}$ and $\text{bot}_{s,k}^{l,c}$ sets from. This module is trained using the first and third terms of the loss function presented in Eq. (2), without multiplying the first term by 2, and with $k_1 = k_3 = HW$. We call this module the discriminative scoring module. We detached the input of this module to prevent misleading loss injection to

the model, as many input parts may be common between the concepts.

2) *Knowledge sharing by concordance loss:* Intuitively, if one LAP layer has found a part of the input as the distinguishing clue for one concept, the proceeding LAP layers should also distinguish the same clue. This fact does not always hold for the previous layers, as they might not have enough understanding to perceive the clue, mainly due to the low receptive field. A human expert can decide whether the receptive field is enough for the LAP layers. In that case, we have used the Jensen-Shannon divergence loss for encouraging the consecutive LAP layers to produce similar maps:

$$\begin{aligned}
\mathcal{JS}(l, s, c) = & \frac{1}{2M_s} \sum_{(i,j); |p_{s,i,j}^{l,c} - p_{s,i,j}^{l+1,c}| > t} \left[\right. \\
& (p_{s,i,j}^{l,c} - p_{s,i,j}^{l+1,c}) \ln \frac{p_{s,i,j}^{l,c}}{p_{s,i,j}^{l+1,c}} + \quad (3) \\
& \left. (p_{s,i,j}^{l+1,c} - p_{s,i,j}^{l,c}) \ln \frac{1 - p_{s,i,j}^{l,c}}{1 - p_{s,i,j}^{l+1,c}} \right],
\end{aligned}$$

where $\mathcal{JS}(l, s, c)$ is the loss for the concept head c of sample s between the LAPs l and $l+1$. The loss is calculated only on the pixels whose importance probabilities in two consecutive LAP layers are more than a specified threshold t . M_s is the number of such pixels in sample s .

Using the Jensen-Shannon loss causes the LAP layers to help each other in finding more clues and the found clues are also more robust. If the receptive field does not suffice in some layer, e.g. l , only the pixels with high importance probabilities of l and low importance probabilities of $l+1$ can be used in the Jensen-Shannon divergence loss. We have applied this loss between each pair of consecutive LAP layers.

D. LAP-Extended Models

LAP is easily pluggable into any convolutional architecture. Pooling and adaptive pooling layers can be replaced directly with LAPs. Strided convolutions can also be replaced by a convolution with the stride of one, proceeding with a LAP with the same kernel size and stride as the convolution's stride. The unique advantage of LAP is that it can be plugged into an already trained model and tuned while other model layers are frozen.

IV. RESULTS

We evaluated the performance and interpretability of LAP-extended models on three datasets from three different domains. To show the general applicability, we adopted two widely used CNN architectures in our experiments, ResNet [15], and Inception-V3 [36]. While both architectures have high performance, they have different core ideas. ResNet is famous for its residual connections that prepare uninterrupted gradient paths to prevent gradient fading. Inception-V3 is known for its multi-resolution analysis by applying kernels of different sizes to the feature map at each network level. We compared our interpretations with three white-box explainer

TABLE I

RESULTS ON THE RSNA DATASET. WE EVALUATED THE MODELS' ACCURACY (ACC.), SENSITIVITY (SENS.), SPECIFICITY (SPEC.), AND BALANCED ACCURACY (BA). LAP-EXTENDED MODELS TRAINED WITH WEAK SUPERVISION (WS) AND INFECTION BOUNDING BOXES (BB) HAVE ACHIEVED HIGHER PERFORMANCES THAN THE VANILLA ONES. ACCURACIES OF LAP PREDICTORS W.R.T. GROUND TRUTH (PREDICTIVITY) AND MODEL'S PREDICTION (FAITHFULNESS) SHOW THEIR EFFECTIVENESS.

| Model | Model performance | | | | LAP predictions | | | | Faithfulness to model prediction | | | |
|--------------|-------------------|-------|-------|-------|------------------|------------------|------------------|------------------|----------------------------------|------------------|------------------|------------------|
| | Acc. | Sens. | Spec. | BA | LAP ₁ | LAP ₂ | LAP ₃ | LAP ₄ | LAP ₁ | LAP ₂ | LAP ₃ | LAP ₄ |
| ResNet 18 | 95.22 | 95.08 | 95.37 | 95.23 | - | - | - | - | - | - | - | - |
| WS-LAP RN18 | 96.58 | 97.07 | 96.05 | 96.56 | 55.48 | 69.76 | 88.11 | 94.41 | 55.86 | 70.14 | 88.6 | 96.09 |
| BB-LAP RN18 | 96.96 | 95.92 | 98.08 | 97 | 54.06 | 86.02 | 95.62 | 96.8 | 53.96 | 85.96 | 96.42 | 98.95 |
| Inception V3 | 96.15 | 95.71 | 96.61 | 96.16 | - | - | - | - | - | - | - | - |
| WS-LAP InV3 | 96.63 | 96.03 | 97.29 | 96.66 | 51.9 | 51.9 | 96.15 | 96.25 | 51.14 | 51.14 | 97.56 | 97.67 |
| BB-LAP InV3 | 96.42 | 96.23 | 96.61 | 96.42 | 51.9 | 93.65 | 96.53 | 96.36 | 51.57 | 94.3 | 99.35 | 99.73 |

methods, Guided Back-propagation (GBP), Guided Grad-CAM (GCC) and Deep Lift (DL). We did our experiments on PyTorch [25] and used the implementations of captum [18]. The experiment setup and results for the datasets are presented in the proceeding sections.

A. RSNA pneumonia detection

RSNA pneumonia detection dataset [1] was published in a Kaggle challenge in 2018. The dataset contains chest X-Ray images of 8851 healthy people, 9555 patients having lung pneumonia, and 11821 patients with other lung abnormalities. The zones related to pneumonia have been specified by experts using bounding boxes. We used the samples related to healthy people and the patients having lung pneumonia in a classification task. We used 81% of the data for training, 9% for validation, and 10% as the test set.

In this task, ResNet 18 and Inception V3 were used as the base architectures. We placed three LAP modules in blocks 2, 3, and 4 of ResNet 18, and maxpool2, Mixed6a, and Mixed7a of Inception V3. Adaptive pooling was also replaced with adaptive LAP in both networks. We used two 1×1 convolution layers with eight hidden channels and one concept head for detecting pneumonia, obligated to be partly active in positive samples and completely inactive in negative ones. As there is only one concept head, there is no need for an aggregation module, and final attention scores are equal to the concept scores. We trained LAP-extended models with two different methods, weak knowledge injection (WS), and experts' knowledge injection (BB). For weak supervision, we used cross-entropy loss on the classification head, concept-discrimination loss (MinAR of 0.1, MaxAR of 0.5, and IAR of 0.1), and Inter-LAPs concordance loss with weights of 1, 0.25 per LAP, and 0.25 per LAP pair respectively. For full supervision, we used cross-entropy loss on the classification head alongside cross-entropy loss on LAPs considering experts' bounding boxes as the ground truth with weights of 1 and 0.25 per LAP respectively. The detail of the loss function is explained further in Appendix A.

We trained the models for 200 epochs, where we observed convergence due to no change in the last 50 epochs. We selected the model related to the epoch with the best performance on validation data as the final model. We used batches of size 64 (32 healthy and 32 pneumonia samples) and the ADAM optimizer with an initial learning rate of 10^{-4} and a decay

coefficient of 10^{-6} in training. The models were trained on a GEFORCE RTX 2080 Ti GPU.

We evaluated the models using four metrics, accuracy, sensitivity, Specificity and Balanced Accuracy (BA). Sensitivity and specificity are recall factors for positive and negative classes, respectively. BA is the average of the recalls which gives a fair metric for imbalanced datasets. The evaluation metrics on test data are presented in Tab. I. In both architectures, the LAP-extended versions have surpassed the performance of the vanilla models.

Each LAP layer can also be used as a standalone predictor. If a LAP has assigned a probability of more than 0.5 to at least one pixel, it means it has found infection in the sample. The prediction of the LAP for these samples is assumed positive and otherwise negative. We evaluated the predictivity of LAP modules as standalone deciders and the accuracy of their faithfulness to the model's decisions. According to Tab. I, as expected, the deeper the layer and the larger its receptive field, the higher the predictivity and the faithfulness. It is also observable that the WS-LAP Inception V3 model is more accurate than the BB-LAP one, while in the case of LAP predictivity, the BB-LAPs in both ResNet 18 and Inception V3, have generally higher accuracies than WS-LAPs, especially in LAP₂. This observation implies that using exact supervision leads to better predictivity in most LAP layers.

To verify the superior performance of our self-interpretation method, we compared the interpretations with three famous white-box explainers, GGC, GBP, and DL. We used experts' bounding boxes as ground truth to evaluate the interpretations of the methods. One of the strong points about our method is its global interpretability, meaning the importance scores have the same scale in all samples, and any score greater than 0.5 is interpreted as important. The other interpretation methods provide relative importance scores and do not provide a cross-sample threshold to distinguish the important pixels from unimportant ones. To find a global threshold for other methods, we normalized each importance map by its maximum value. Then we trained a binary linear classifier based on normalized scores to discriminate the pixels under bounding boxes from the others in the validation set (More details are available in Appendix B). We used the classifier's threshold to binarize the normalized score maps of the test data. We used intersection over union (IoU) between the binarized interpretation maps and the ground truth bounding boxes to compare

TABLE II
IOUs OF INFECTION BOUNDING BOXES AND BINARIZED INTERPRETATION
MAPS OF DIFFERENT INTERPRETATION METHODS WITH TWO
BINARIZATION APPROACHES.

| Model | DL | GGC | GBP | LAP |
|--------------------------------------|-------|-------|-------|--------------|
| Binarization by Thresholding | | | | |
| WS-LAP RN18 | 24.63 | 16.03 | 19.13 | 36.25 |
| BB-LAP RN18 | 27.06 | 15.74 | 18.88 | 46.48 |
| WS-LAP InV3 | 26.01 | 22.26 | 25.92 | 31.96 |
| BB-LAP InV3 | 29.69 | 16.22 | 17.05 | 46.91 |
| Binarization by Top-Scored Selection | | | | |
| WS-LAP RN18 | 35.91 | 23.15 | 24.09 | 43.98 |
| BB-LAP RN18 | 41.73 | 22.38 | 22.1 | 58.21 |
| WS-LAP InV3 | 40.3 | 32.26 | 32.43 | 40.31 |
| BB-LAP InV3 | 46.09 | 22.08 | 21.38 | 59.37 |

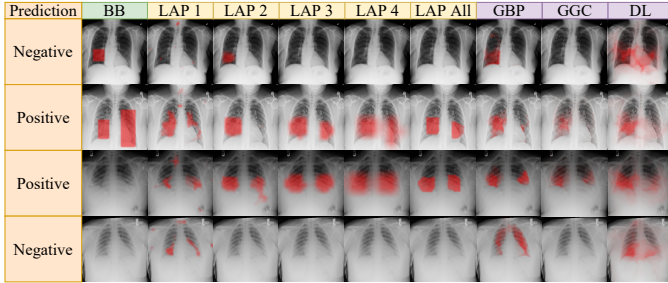


Fig. 4. Examples of BB-LAP Inception V3 interpretations (LAPs) compared to RSNA bounding boxes (BB) and other interpretation methods (GBP, GGC, DL) on RSNA.

the interpretation methods (**Binarization by Thresholding**). As observed in Tab. II, our method has a significantly higher performance than the other methods in both WS-LAP and BB-LAP models. We also adopted another technique for binarizing the infection maps (**Binarization by Top-Scored Selection**). As ground truth bounding boxes are available, we selected as many top-scored pixels as the bounding boxes area of each sample. LAP achieved a higher IOU than other methods in this evaluation too. We visualized the interpretations of different methods over four examples for BB-LAP Inception V3 in Fig. 4. As this figure presents, LAP interpretations are faithful to the model’s prediction, while GBP and DL have failed to do so. In the true-positive decisions of the model, LAP interpretations have an acceptable overlap with infection bounding boxes, while GGC has not been successful in all cases. Details of integrating LAPs (LAP All) and examples of the other models are provided in Appendices C and D, respectively.

B. Large-scale CelebFaces Attributes (CelebA)

To explore the general applicability of our method, we investigated its effectiveness in a different domain, using Large-scale CelebFaces Attributes (CelebA) Dataset [20]. CelebA dataset is a face attributes detection dataset containing 40 face attributes of celebrity images. We applied binary classification on the smile attribute of this dataset. The dataset consists of 202,599 samples. We randomly selected 70%, 10%, and 20% of the data for training, validation, and test sets, respectively.

In this task, ResNet 18 and Inception V3 were used as base architectures, and the LAPs were placed as described

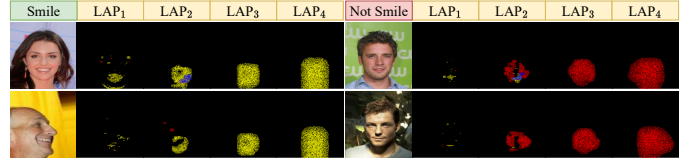


Fig. 5. Examples of LAP Inception V3 interpretations on CelebA. Yellow, red, and blue points indicate smiling, not smiling, and common concept heads, respectively (See Appendix D for examples on LAP ResNet 18).

in Sec. IV-A. We used two 1×1 convolution layers with eight hidden channels and three heads to generate concept-wise scores. The two first concept heads refer to negative and positive classes, each obligated to be partially active in its respective class samples and completely inactive otherwise. The third head was added to highlight the common effective pixels with a low concept-discriminability due to the lack of receptive field. The sum of the three heads’ scores was used as the aggregation module to generate final attention scores. We trained LAP-extended models with our proposed weak knowledge injection method. We used the same loss as Sec. IV-A with different limits (MinAR of 0.02, MaxAR of 0.2, and IAR of 0.01 for the first two heads and MaxAR of 0.1, without MinAR and IAR for the common concept head). We trained the networks for 12 epochs, where we observed convergence. The other training hyper-parameters were also the same as in Sec. IV-A.

The evaluation metrics on the test set are presented in Tab. III. In both architectures, the LAP-extended versions have surpassed the performance of the vanilla ones. We also evaluated LAPs’ performance and faithfulness as standalone predictors. In this experiment, we took the class with the higher sum of importance scores as the final prediction of the LAP module. We can observe that LAP layers have a very high faithfulness to the model. Moreover, we can use LAPs to diagnose the model’s performance throughout its depth. For example, LAP₂ in LAP Inception V3 has a very close accuracy to the final classifier and higher accuracy than the vanilla version. So we can drop the proceeding layers to have a much smaller and faster model in the inference stage without performance loss.

The LAP interpretations are visualized for four examples in Fig. 5. As expected, the interpretations are concentrated around the lips. LAPs also have been successful to discriminate the concepts.

C. Imagenet

In this experiment, we explored the adaptability of our LAPs in already trained models. We chose the ImageNet classification task [29] to assess whether the LAPs can handle interpretations of objects with high variance in size. We used pre-trained ResNet 50 from the torchvision model zoo [22] as the base architecture. Generally, the objects of the ImageNet dataset may have a larger size than the receptive field of the first three layers. Therefore, we only used a LAP in the fourth layer. We used a 1×1 convolution layer with 1000 heads, each obligated to be partly active in its respective class samples and

TABLE III

RESULTS ON THE CELEBA DATASET. WE EVALUATED THE MODELS' ACCURACY (ACC.), SENSITIVITY (SENS.), SPECIFICITY (SPEC.), AND BALANCED ACCURACY (BA). WE COMPARED THE ORIGINAL RESNET 18 AND INCEPTION V3 MODELS WITH LAP-EXTENDED ONES. THE RESULTS SHOW THAT THE LAP-EXTENDED MODELS HAVE ACHIEVED A HIGHER PERFORMANCE.

| Model | Model performance | | | | LAP predictions | | | | Faithfulness to model prediction | | | |
|--------------|-------------------|-------|-------|-------|------------------|------------------|------------------|------------------|----------------------------------|------------------|------------------|------------------|
| | Acc. | Sens. | Spec. | BA | LAP ₁ | LAP ₂ | LAP ₃ | LAP ₄ | LAP ₁ | LAP ₂ | LAP ₃ | LAP ₄ |
| ResNet 18 | 92.82 | 90.8 | 94.7 | 92.75 | - | - | - | - | - | - | - | - |
| LAP RN18 | 92.86 | 91.6 | 94.04 | 92.82 | 52.32 | 71.9 | 88.73 | 92.57 | 53.31 | 73.04 | 91.34 | 97.78 |
| Inception V3 | 92.8 | 91.7 | 93.83 | 92.77 | - | - | - | - | - | - | - | - |
| LAP InV3 | 92.98 | 91.38 | 94.47 | 92.92 | 58.2 | 92.14 | 92.92 | 92.9 | 57.58 | 95.91 | 99.39 | 99.22 |

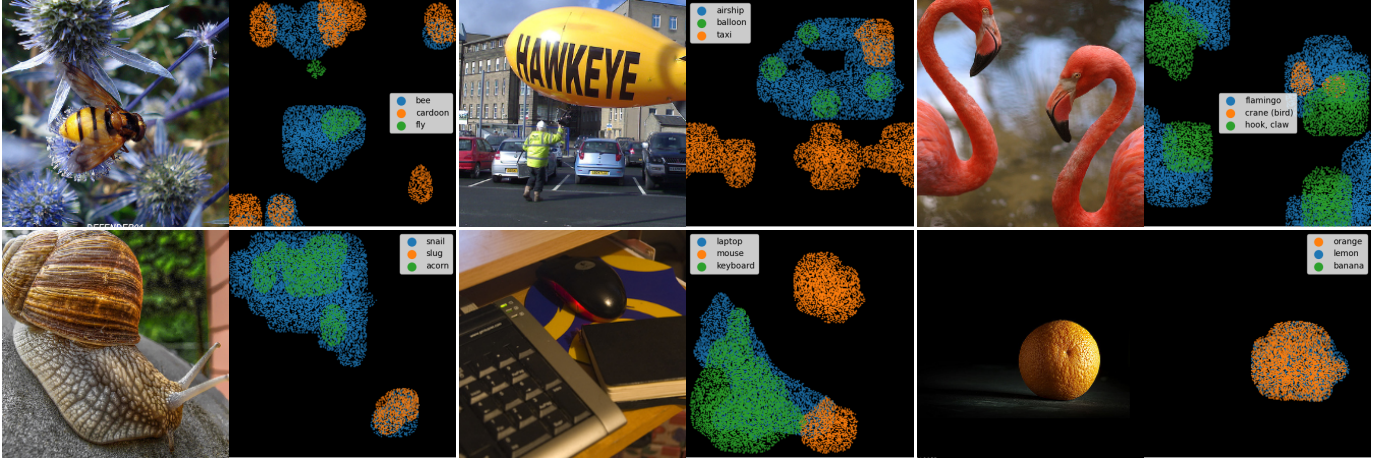


Fig. 6. Examples of LAP ResNet 50 interpretation on ImageNet. Different concept heads are illustrated by different colors. The legend shows the top-3 classes in order based on the model's predictions. Note that in the last example (orange), the probability of banana class has been 0.001, and its respective concept head has not been active too (See Appendix D for more examples).

TABLE IV

RESULTS ON THE IMAGENET DATASET. WE EVALUATED MODELS' TOP-1 AND TOP-5 ACCURACIES. NFT: NOT FINETUNED - FT: FINETUNED

| Model | Top-1 Acc. | Top-5 Acc. |
|---------------------|------------|------------|
| ResNet 50 | 76.13 | 92.86 |
| LAP ResNet 50 (NFT) | 75.87 | 92.74 |
| LAP ResNet 50 (FT) | 76.16 | 92.85 |

completely inactive otherwise. We used a 1×1 convolution layer as the aggregation module to generate the final attention scores. We used our proposed weakly supervised loss (MinAR and IAR of 0.01, without MaxAR) with a factor of 0.125 beside the main cross-entropy loss. We first trained only the LAP module while other parameters were frozen for two epochs using the ADAM optimizer with an initial learning rate of 10^{-4} and a decay coefficient of 10^{-6} . Then, we finetuned the fourth layer (containing the LAP) and the fully connected layer of the ResNet 50 using a stochastic gradient descent optimizer with an initial learning rate of 10^{-3} and a decay coefficient of 10^{-6} for three epochs. The performances of the original model, the version with its LAP trained, and the final tuned one are presented in Tab. IV. It is observable that LAP has been able to adapt itself to the model while the performance is slightly improved.

The interpretation of the class heads according to the top-3 predictions of the model is illustrated in Fig. 6. As we can observe, the LAP shows that the model concentrates on the sample's different objects, and it is visually faithful to

the model's prediction. It also can illustrate the model's bias for predicting a class. In the first example, the flower has been considered as a clue of the bee class. In the second example, the model has assigned a high probability to the taxi class because the sample contains some cars and a yellow object, both highlighted by the taxi concept head. In the third example, the model has considered the curvatures of the neck of flamingos as some hooks. The LAP also explains why the model has assigned a high probability to the top-3 classes. In the first example, the bee's head is similar to a fly. In the fourth image, the pattern and color of the snail shell have been similar to an acorn.

V. CONCLUSION

This paper introduced Local Attention Pool (LAP), a concept-wise attention-based pooling method pluggable into any convolutional architecture, even an already trained one. We showed LAPs accommodate models with self-interpretability without performance loss. Furthermore, LAP attention maps proved their ability in explaining the model's behavior faithful to its predictions compared to other explainers. They also can be used as standalone predictors. Their architecture can adapt to different domains and discriminate their concepts by weak or full supervision and knowledge sharing. In the future, we plan to use LAPs on tasks other than classification and improve the explainability by addressing the issues with receptive-field dependency.

REFERENCES

- [1] Pneumonia detection challenge database (2018). Accessed April 10, 2021. [5](#)
- [2] Samira Abnar and Willem Zuidema. Quantifying attention flow in transformers. Association for Computational Linguistics, 2020. [2](#)
- [3] Dzmitry Bahdanau, Kyunghyun Cho, and Yoshua Bengio. Neural machine translation by jointly learning to align and translate. *arXiv preprint arXiv:1409.0473*, 2014. [1](#)
- [4] Alexander Binder, Grégoire Montavon, Sebastian Lapuschkin, Klaus-Robert Müller, and Wojciech Samek. Layer-wise relevance propagation for neural networks with local renormalization layers. In *International Conference on Artificial Neural Networks*, pages 63–71. Springer, 2016. [2](#)
- [5] Rich Caruana, Yin Lou, Johannes Gehrke, Paul Koch, Marc Sturm, and Noemie Elhadad. Intelligible models for healthcare: Predicting pneumonia risk and hospital 30-day readmission. In *Proceedings of the 21th ACM SIGKDD international conference on knowledge discovery and data mining*, pages 1721–1730, 2015. [1](#)
- [6] Hila Chefer, Shir Gur, and Lior Wolf. Generic attention-model explainability for interpreting bi-modal and encoder-decoder transformers. In *Proceedings of the IEEE/CVF International Conference on Computer Vision (ICCV)*, pages 397–406, October 2021. [2](#)
- [7] Hila Chefer, Shir Gur, and Lior Wolf. Transformer interpretability beyond attention visualization. In *Proceedings of the IEEE/CVF Conference on Computer Vision and Pattern Recognition (CVPR)*, pages 782–791, June 2021. [2](#)
- [8] Xi Chen, Yan Duan, Rein Houthoofd, John Schulman, Ilya Sutskever, and Pieter Abbeel. Infogan: Interpretable representation learning by information maximizing generative adversarial nets. In *Proceedings of the 30th International Conference on Neural Information Processing Systems*, pages 2180–2188, 2016. [1](#)
- [9] Mengnan Du, Ninghao Liu, and Xia Hu. Techniques for interpretable machine learning. *Communications of the ACM*, 63(1):68–77, 2019. [1](#)
- [10] Alex A Freitas. Comprehensive classification models: a position paper. *ACM SIGKDD explorations newsletter*, 15(1):1–10, 2014. [1](#)
- [11] Ziteng Gao, Limin Wang, and Gangshan Wu. Lip: Local importance-based pooling. In *Proceedings of the IEEE/CVF International Conference on Computer Vision*, pages 3355–3364, 2019. [2](#)
- [12] Leilani H Gilpin, David Bau, Ben Z Yuan, Ayesha Bajwa, Michael Specter, and Lalana Kagal. Explaining explanations: An overview of interpretability of machine learning. In *2018 IEEE 5th International Conference on data science and advanced analytics (DSAA)*, pages 80–89. IEEE, 2018. [1](#)
- [13] Bryce Goodman and Seth Flaxman. European union regulations on algorithmic decision-making and a “right to explanation”. *AI magazine*, 38(3):50–57, 2017. [1](#)
- [14] Ran Gu, Guotai Wang, Tao Song, Rui Huang, Michael Aertsen, Jan Deprest, Sébastien Ourselin, Tom Vercauteren, and Shaoting Zhang. Ca-net: Comprehensive attention convolutional neural networks for explainable medical image segmentation. *IEEE Transactions on Medical Imaging*, 2020. [2](#)
- [15] Kaiming He, Xiangyu Zhang, Shaoqing Ren, and Jian Sun. Deep residual learning for image recognition. In *Proceedings of the IEEE conference on computer vision and pattern recognition*, pages 770–778, 2016. [4](#)
- [16] Been Kim, Martin Wattenberg, Justin Gilmer, Carrie Cai, James Wexler, Fernanda Viegas, et al. Interpretability beyond feature attribution: Quantitative testing with concept activation vectors (tcav). In *International conference on machine learning*, pages 2668–2677. PMLR, 2018. [1](#)
- [17] Diederik P Kingma and Max Welling. Auto-encoding variational bayes. *arXiv preprint arXiv:1312.6114*, 2013. [1](#)
- [18] Narine Kokhlikyan, Vivek Miglani, Miguel Martin, Edward Wang, Bilal Alsallakh, Jonathan Reynolds, Alexander Melnikov, Natalia Kliushkina, Carlos Araya, Siqi Yan, and Orion Reblitz-Richardson. Captum: A unified and generic model interpretability library for pytorch, 2020. [5](#)
- [19] Alexander Kolesnikov, Alexey Dosovitskiy, Dirk Weissenborn, Georg Heigold, Jakob Uszkoreit, Lucas Beyer, Matthias Minderer, Mostafa Dehghani, Neil Houlsby, Sylvain Gelly, Thomas Unterthiner, and Xi-aohua Zhai. An image is worth 16x16 words: Transformers for image recognition at scale. 2021. [2](#)
- [20] Ziwei Liu, Ping Luo, Xiaoqiang Wang, and Xiaoou Tang. Deep learning face attributes in the wild. In *Proceedings of International Conference on Computer Vision (ICCV)*, December 2015. [6](#)
- [21] Jiasen Lu, Jianwei Yang, Dhruv Batra, and Devi Parikh. Hierarchical question-image co-attention for visual question answering. *Advances in neural information processing systems*, 29:289–297, 2016. [1](#)
- [22] Sébastien Marcel and Yann Rodriguez. Torchvision the machine-vision package of torch. In *Proceedings of the 18th ACM international conference on Multimedia*, pages 1485–1488, 2010. [6](#)
- [23] Arnab Kumar Mondal, Arnab Bhattacharjee, Parag Singla, and Prathosh AP. xViTCOS: Explainable vision transformer based COVID-19 screening using radiography. July 2021. [2](#)
- [24] Chris Olah, Alexander Mordvintsev, and Ludwig Schubert. Feature visualization. *Distill*, 2017. <https://distill.pub/2017/feature-visualization>. [3](#)
- [25] Adam Paszke, Sam Gross, Francisco Massa, Adam Lerer, James Bradbury, Gregory Chanan, Trevor Killeen, Zeming Lin, Natalia Gimelshein, Luca Antiga, Alban Desmaison, Andreas Kopf, Edward Yang, Zachary DeVito, Martin Raison, Alykhan Tejani, Sasank Chilamkurthy, Benoit Steiner, Lu Fang, Junjie Bai, and Soumith Chintala. Pytorch: An imperative style, high-performance deep learning library. In H. Wallach, H. Larochelle, A. Beygelzimer, F. d’Alché-Buc, E. Fox, and R. Garnett, editors, *Advances in Neural Information Processing Systems 32*, pages 8024–8035. Curran Associates, Inc., 2019. [5](#)
- [26] Mensah Kwabena Patrick, Adebayo Felix Adekoya, Ayidzoe Abra Mighty, and Baagyire Y Edward. Capsule networks—a survey. *Journal of King Saud University-computer and information sciences*, 2019. [2](#)
- [27] F. Pedregosa, G. Varoquaux, A. Gramfort, V. Michel, B. Thirion, O. Grisel, M. Blondel, P. Prettenhofer, R. Weiss, V. Dubourg, J. Vanderplas, A. Passos, D. Cournapeau, M. Brucher, M. Perrot, and E. Duchesnay. Scikit-learn: Machine learning in Python. *Journal of Machine Learning Research*, 12:2825–2830, 2011. [9](#)
- [28] Marco Tulio Ribeiro, Sameer Singh, and Carlos Guestrin. “why should i trust you?” explaining the predictions of any classifier. In *Proceedings of the 22nd ACM SIGKDD international conference on knowledge discovery and data mining*, pages 1135–1144, 2016. [2](#)
- [29] Olga Russakovsky, Jia Deng, Hao Su, Jonathan Krause, Sanjeev Satheesh, Sean Ma, Zhiheng Huang, Andrej Karpathy, Aditya Khosla, Michael Bernstein, Alexander C. Berg, and Li Fei-Fei. ImageNet Large Scale Visual Recognition Challenge. *International Journal of Computer Vision (IJCV)*, 115(3):211–252, 2015. [6](#)
- [30] Sara Sabour, Nicholas Frosst, and Geoffrey E Hinton. Dynamic routing between capsules. *arXiv preprint arXiv:1710.09829*, 2017. [1](#)
- [31] Ramprasaath R Selvaraju, Michael Cogswell, Abhishek Das, Ramakrishna Vedantam, Devi Parikh, and Dhruv Batra. Grad-cam: Visual explanations from deep networks via gradient-based localization. In *Proceedings of the IEEE international conference on computer vision*, pages 618–626, 2017. [2](#)
- [32] Avanti Shrikumar, Peyton Greenside, and Anshul Kundaje. Learning important features through propagating activation differences. In *International Conference on Machine Learning*, pages 3145–3153. PMLR, 2017. [2](#)
- [33] Karen Simonyan, Andrea Vedaldi, and Andrew Zisserman. Deep inside convolutional networks: Visualising image classification models and saliency maps. *arXiv preprint arXiv:1312.6034*, 2013. [2](#)
- [34] Leon Sixt, Maximilian Granz, and Tim Landgraf. When explanations lie: Why many modified bp attributions fail. In *International Conference on Machine Learning*, pages 9046–9057. PMLR, 2020. [1](#)
- [35] Jost Tobias Springenberg, Alexey Dosovitskiy, Thomas Brox, and Martin Riedmiller. Striving for simplicity: The all convolutional net. *arXiv preprint arXiv:1412.6806*, 2014. [2](#)
- [36] Christian Szegedy, Vincent Vanhoucke, Sergey Ioffe, Jon Shlens, and Zbigniew Wojna. Rethinking the inception architecture for computer vision. In *Proceedings of the IEEE conference on computer vision and pattern recognition*, pages 2818–2826, 2016. [4](#)
- [37] Gilles Vandewiele, Olivier Janssens, Femke Ongenaes, Filip De Turck, and Sofie Van Hoecke. Genesim: genetic extraction of a single, interpretable model. In *NIPS2016, the 30th Conference on Neural Information Processing Systems*, pages 1–6, 2016. [2](#)
- [38] Tianfu Wu, Wei Sun, Xilai Li, Xi Song, and Bo Li. Towards interpretable r-cnn by unfolding latent structures. *arXiv preprint arXiv:1711.05226*, 2017. [1](#)
- [39] Sen Yang, Zhibin Quan, Mu Nie, and Wankou Yang. Transpose: Keypoint localization via transformer. In *IEEE/CVF International Conference on Computer Vision (ICCV)*, 2021. [2](#)
- [40] Quanzeng You, Hailin Jin, Zhaowen Wang, Chen Fang, and Jiebo Luo. Image captioning with semantic attention. In *Proceedings of the IEEE conference on computer vision and pattern recognition*, pages 4651–4659, 2016. [1](#)
- [41] Quanshi Zhang, Ying Nian Wu, and Song-Chun Zhu. Interpretable convolutional neural networks. In *Proceedings of the IEEE Conference on Computer Vision and Pattern Recognition*, pages 8827–8836, 2018. [1](#)
- [42] Xin Zhang, Liangxiu Han, Wenyong Zhu, Liang Sun, and Daoqiang Zhang. An explainable 3d residual self-attention deep neural network for joint atrophy localization and alzheimer’s disease diagnosis using

APPENDIX

A. Fully supervised LAP loss on RSNA

The loss function for full supervision is very similar to the weakly supervised concept discrimination loss of section 3.3.1. We used experts' annotated bounding boxes as the ground truth for active pixels for the first term. Because all the areas under a bounding box may not belong to infection zones, we applied the loss on half of the pixels with higher importance probability within the box only. All the zones out of the bounding boxes correspond to non-infection areas. We applied the second term to all of them. The third term was used similarly as the weakly supervised loss.

B. Finding global threshold for binarizing white-box explainer's scores

To find a global threshold for other explainer methods, we first normalized each importance map by its maximum value according to their papers. Then we created a dataset from the normalized pixel-wise interpretation scores over the validation samples. We assigned the positive label to all the pixels under experts' annotated boxes and negative to the others. We used RidgeClassifier of sklearn [27] for the classification of the pixels. Due to the large number of pixels, we used the lsqr solver with a tolerance of 10^{-3} , alpha of 0.01, and set the maximum iterations to 100. We also used balanced weighting to address the issue with the highly imbalanced dataset. We used the point with the prediction label equal to zero as the threshold for binarization. We applied this method for each trained model separately and used the resulting threshold to evaluate the model's interpretations.

C. Integrating LAPs scores to one unified interpretation map

LAPs can be viewed as a sequence of information. The initial LAPs, due to the lower receptive field, cannot capture enough information. Therefore, they are likely to make more mistakes. Some pixels may have been assumed to be important but were found unimportant in the later layers and vice versa. But because of the low receptive field, they are more precise and give maps of higher resolutions. We devised an algorithm to correct interpretations from the final LAP layers recursively to the initial layers. In this way, we can have both accuracy and resolution. Starting from the last LAP, L , we correct the LAP before, $L-1$, using this scheme. When resizing the score map of L to the size of $L-1$ by nearest transformation, each pixel of L corresponds to some of the pixels of $L-1$. Considering one pixel of L , X_L and the set of corresponding pixels in $L-1$, CX_L , if X_L was active, had an importance probability over 0.5, at least one pixel in the corresponding zone must have been responsible. If any of the CX_L was active, we gave the entire credit to the active pixel. Otherwise, the reason for the activation of X_L had not been clear from the previous LAP, so we assigned the credit to all of them. Using this scheme, we prune the produced importance map from the last LAP, which

is expected to be the most accurate, to the first. For ranking the pixels in Binarization by Top-Scored Selection in section 4.1, we simply added the scores of all LAPs.

D. More examples of LAP interpretations

Due to the limitation on the number of pages in the main paper, we have provided more images interpreted with LAP for each of the three datasets in Figs. 7, 8 and 9.

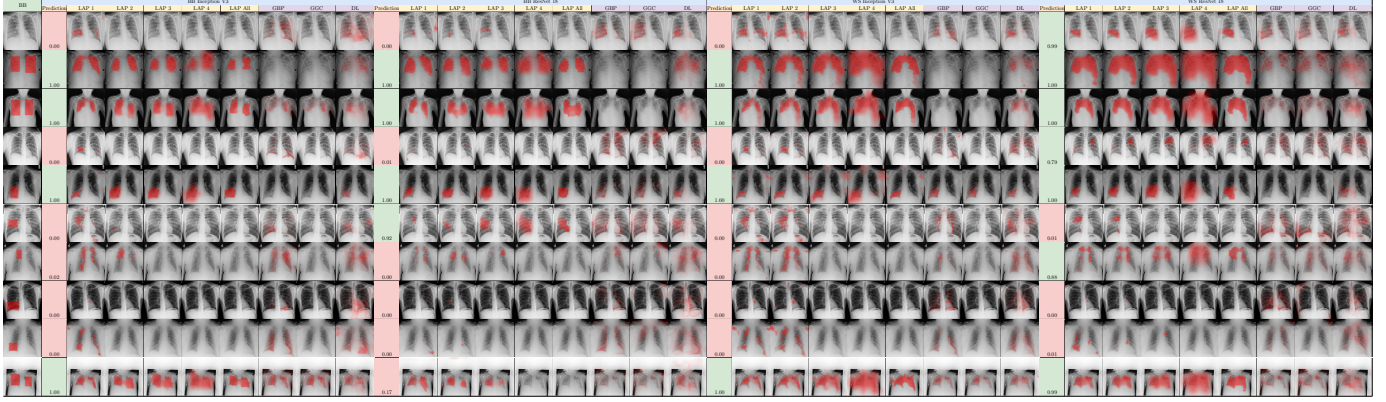


Fig. 7. Examples of all models' interpretations (LAPs) compared to RSNA bounding boxes (BB) and other interpretations methods (GBP, GGC, DL) on the RSNA dataset. The probability assigned by each model is presented too.

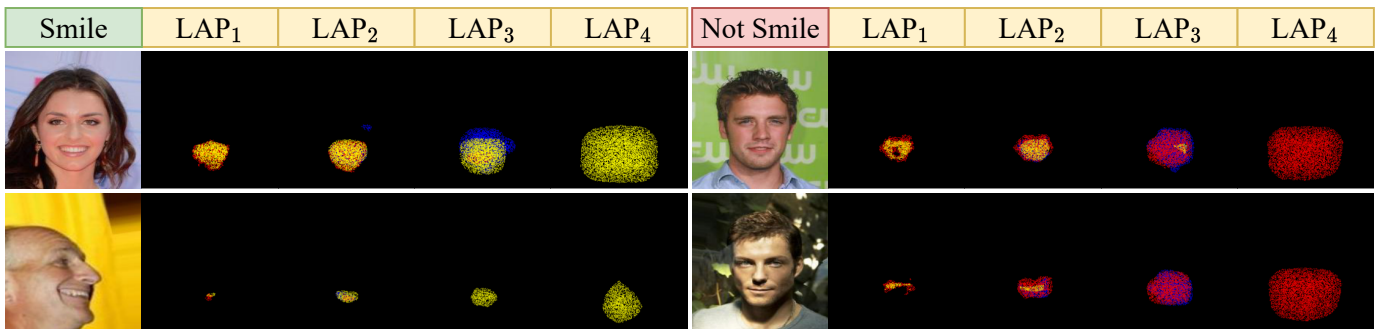


Fig. 8. Examples of LAP ResNet 18 on CelebA dataset.



Fig. 9. Further Concept-wise interpretation Examples of LAP ResNet 50 on ImageNet dataset. For each example, concept heads related to top-5 predictions of the model are illustrated separately. The probability assigned by the model for each concept head is presented too.